nature materials

LETTERS

https://doi.org/10.1038/s41563-017-0010-4

Atomic scale imaging of magnetic circular dichroism by achromatic electron microscopy

Zechao Wang[1], Amir H. Tavabi[2], Lei Jin[2], Ján Rusz[3], Dmitry Tyutyunnikov[3], Hanbo Jiang[1], Yutaka Moritomo[4], Joachim Mayer[2,5], Rafal E. Dunin-Borkowski[2], Rong Yu[1], Jing Zhu[1] and Xiaoyan Zhong[1]*

In order to obtain a fundamental understanding of the interplay between charge, spin, orbital and lattice degrees of freedom in magnetic materials and to predict and control their physical properties[1-3], experimental techniques are required that are capable of accessing local magnetic information with atomic-scale spatial resolution. Here, we show that a combination of electron energy-loss magnetic chiral dichroism[4] and chromatic-aberration-corrected transmission electron microscopy, which reduces the focal spread of inelastically scattered electrons by orders of magnitude when compared with the use of spherical aberration correction alone, can achieve atomic-scale imaging of magnetic circular dichroism and provide element-selective orbital and spin magnetic moments atomic plane by atomic plane. This unique capability, which we demonstrate for Sr_2FeMoO_6, opens the door to local atomic-level studies of spin configurations in a multitude of materials that exhibit different types of magnetic coupling, thereby contributing to a detailed understanding of the physical origins of magnetic properties of materials at the highest spatial resolution.

The ability to resolve local spin and orbital magnetic moments in materials with atomic spatial resolution has been a long-standing goal of magnetic characterization. Two of the leading techniques in spatially resolved magnetic imaging are spin-polarized scanning tunnelling microscopy[5,6] and magnetic exchange force microscopy[7], which can be used to map surface spin structures with atomic spatial resolution. However, they are sensitive only to surface layers of atoms, and little information can be obtained about bulk or buried materials. An alternative technique is X-ray magnetic circular dichroism (XMCD) using synchrotron-based X-ray photoelectron emission microscopy, which provides element specificity and depth information of around 5 nm (ref. [8]). However, the spatial resolution of the magnetic contrast detected by left and right circularly polarized X-rays is only about 15 nm (ref. [9]), reaching 7 nm via spectro-ptychography[10]. Although off-axis electron holography in the transmission electron microscope (TEM) can be used to record nanometre-scale information about in-plane magnetic moments, it has also not yet demonstrated magnetic characterization on the atomic scale[11].

Electron energy-loss magnetic chiral dichroism (EMCD) is analogous to the well-established XMCD technique[4]. It provides quantitative element-selective information about spin and orbital magnetic moments in crystalline materials from electron energy-loss (EEL) spectra measured at core-level edges of magnetic elements[12–15]. As a result of the very short de Broglie wavelength and penetration of high-energy electrons, EMCD offers better spatial resolution and depth sensitivity than XMCD[16,17]. When using convergent illumination, the spatial resolution of EMCD depends on the size of the focused electron beam. However, the strength of the signal decreases with increasing convergence angle[18]. By using either an atomic-sized electron probe with a controlled beam shift[19] or a customized phase distribution[20,21], statistical EMCD-like components have been measured. However, true mapping of magnetic circular dichroism (MCD) at the atomic level has not yet been achieved.

Here, we demonstrate an approach that can be used to access MCD atomic plane by atomic plane on an individual basis under parallel beam illumination (PBI) conditions. The approach is based on spatially resolved electron energy-loss spectroscopy (SREELS), which was originally proposed in ref. [22] and subsequently developed for chemical shift analysis[23,24]. In SREELS, the intensity in a conjugate image plane at the position of the spectrometer entrance aperture (Fig. 1a) is dispersed as a function of energy (Fig. 1d). In the energy-dispersive plane, each column along the horizontal direction in the image corresponds to the same energy loss, while each row along the vertical direction corresponds to an area that has the same y value on the specimen. As both energy-loss and spatial information are recorded in parallel, one can in principle achieve high energy resolution along the horizontal direction and high spatial resolution along the vertical direction simultaneously.

Most importantly, chromatic aberration (C_C) normally introduces significant contrast delocalization in real space and degrades image quality as a result of changes in defocus with energy loss. With the recent advent of C_C correction[25,26], the change in defocus of inelastically scattered electrons that have a total energy width as large as 400 eV can be limited to 1 nm, which is crucial for achieving atomic-scale spatial resolution and high energy resolution under PBI conditions with a small convergence angle in an achromatic SREELS image. Spherical aberration (C_S) correction and the choice of an optimized defocus are also important to minimize delocalization, since the contrast in an elastic wavefunction is preserved in an inelastic wave due to the delocalized nature of transition potentials[27].

In this paper, we achieve atomic-resolution MCD under PBI conditions atomic plane by atomic plane in one direction by using a

[1]National Center for Electron Microscopy in Beijing, Key Laboratory of Advanced Materials (MOE), The State Key Laboratory of New Ceramics and Fine Processing, School of Materials Science and Engineering, Tsinghua University, Beijing, China. [2]Ernst Ruska-Centre for Microscopy and Spectroscopy with Electrons and Peter Grünberg Institute, Forschungszentrum Jülich GmbH, Jülich, Germany. [3]Department of Physics and Astronomy, Uppsala University, Uppsala, Sweden. [4]Graduate School of Pure & Applied Science and Faculty of Pure & Applied Science, University of Tsukuba, Tsukuba, Japan. [5]Central Facility for Electron Microscopy, RWTH Aachen University, Aachen, Germany. *e-mail: xyzhong@mail.tsinghua.edu.cn

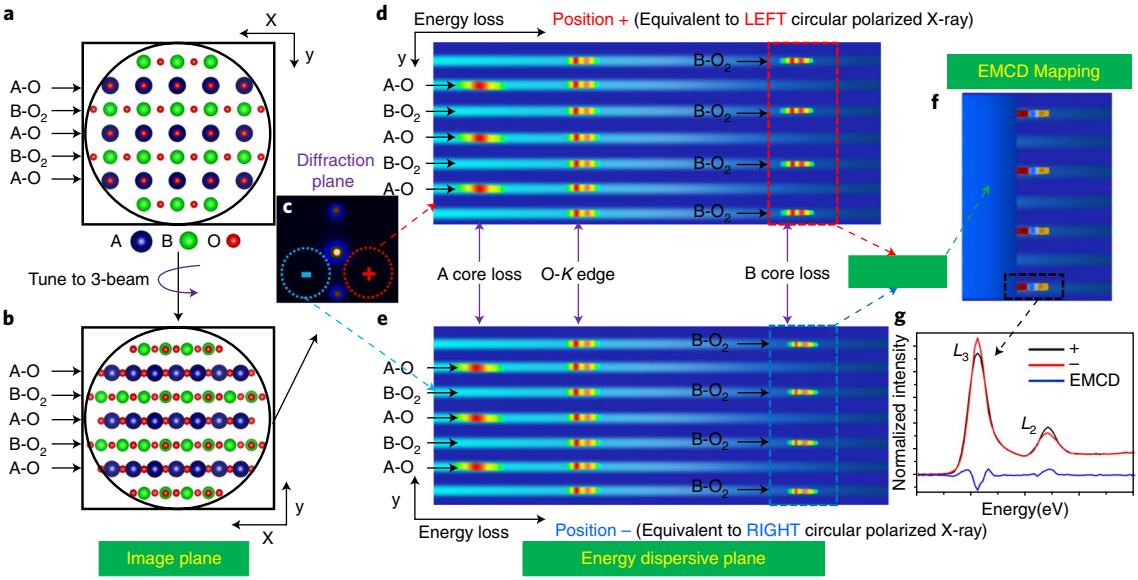

Fig. 1 | Schematic diagram illustrating atomic-scale imaging of magnetic circular dichroism (MCD). a, Atomic structure of a perovskite oxide with the formula ABO_3 at a [110] zone axis with the (002) crystallographic planes parallel to the *x* direction of the camera. **b**, Atomic structure of ABO_3 at a three-beam condition (3BC) with the (002) systematic reflections excited and the (002) crystallographic planes strictly parallel to the incident electron beam direction under PBI. **c**, Electron diffraction pattern at a 3BC with the (002) systematic reflections excited. Positive and negative Thales positions of the objective aperture (OA) corresponding to opposite chirality are labelled '+' in red and '−' in blue, respectively. **d**,**e**, Achromatic SREELS images in the energy-dispersive plane with the OA placed at the positive and negative positions, respectively. **f**, Atomic-scale imaging of MCD achieved by subtracting the SREELS image acquired at the '+' position from that acquired at the '−' position. **g**, MCD spectrum of an individual atomic plane extracted from **f**.

combination of C_C correction, SREELS and EMCD. Figure 1 shows a schematic diagram of the basis of the technique illustrated for a perovskite oxide with the formula ABO_3.

In Fig. 1a, the ABO_3 crystal is viewed along the [110] zone axis, with the (002) crystallographic planes oriented parallel to the *x* direction of the charge-coupled device (CCD) camera. The specimen is tilted to a 3BC with the (002) crystallographic planes remaining strictly parallel to the incident electron beam direction (Fig. 1b). Figure 1c shows the corresponding electron diffraction pattern. The objective aperture (OA) is placed at the Thales positions, which are labelled '+' in red and '−' in blue, correspond to opposite chirality[4] and are equivalent to left and right circularly polarized X-rays in XMCD, respectively. Figure 1d,e shows achromatic SREELS images in the energy-dispersive plane recorded with the OA placed at the '+' and '−' positions, respectively. As a result of C_C correction, the energy-loss electrons are well focused across the entire energy window in the achromatic SREELS image. For ABO_3, the core-loss edges of the A cations, B cations and O anions can then be distinguished in each atomic plane under PBI conditions, and both energy-loss information for the selected chirality and atomic-scale spatial information along the [001] direction can be recorded simultaneously. By subtracting the SREELS image acquired at the '+' position from that acquired at the '−' position, atomic-scale imaging of MCD is achieved (Fig. 1f) and the EMCD spectra of individual atomic planes (Fig. 1g) can be extracted for quantitative analysis of magnetic parameters.

Figure 2a shows an experimental achromatic SREELS image of the double perovskite Sr_2FeMoO_6 (SFMO) recorded in a 3BC with the (004) systematic reflections excited and without using an OA. The crystallographic and magnetic structure of SFMO is shown in Fig. 2b and in Methods. The tails of the Sr *M* edge along the (004) Sr-O atomic planes have a 4 Å spacing and are marked by blue arrows. The intensity of the O *K* edge is visible not only in the Sr-O (004) atomic planes but also in the Fe/Mo-O (004) atomic planes. On following the tail of the O *K* edge along the Fe/Mo-O (004) atomic planes, significant intensity is visible at the Fe $L_{3,2}$ edge localized on the Fe/Mo-O (004) atomic planes. Figure 2c reveals the arrangements of all atoms in SFMO along the $[110]_{pc}$ zone axis by the negative spherical aberration imaging technique, which is consistent with its corresponding structure model (see the inset of Fig. 2c). An aberration-corrected high-angle annular dark field scaning transmission electron microscopy (HAADF-STEM) image and an atomic-scale energy-dispersive X-ray (EDX) map show perfect chemical ordering in the SFMO (Supplementary Fig. S1). Figure 2d,e shows normalized background-subtracted SREELS images recorded at the O *K* edge and the Fe $L_{2,3}$ edge, respectively, after processing via principal component analysis (PCA). The vertical spacing of 2 Å in the SREELS image at the O *K* edge is consistent with the interplanar spacing between adjacent Fe/Mo-O (004) and Sr-O (004) atomic planes (Fig. 2c), as indicated by arrows, while the vertical spacing of 4 Å at the Fe $L_{2,3}$ edge corresponds to the interplanar spacing of the Fe/Mo-O (004) atomic planes. The achromatic SREELS image of SFMO recorded in a 3BC with the (004) systematic reflections excited clearly resolves chemical ordering along the [001] direction of SFMO on the atomic scale. The EELS spectra from individual Fe/Mo-O (004) and Sr-O (004) atomic planes are recorded simultaneously with atomic spatial resolution.

Achromatic SREELS images of 14-nm-thick SFMO in a 3BC with the (004) systematic reflections excited were recorded with the OA located at the positive (Fig. 3a) and negative (Fig. 3b) positions in the diffraction plane, as shown schematically in Fig. 1c. The vertical spacing of 4 Å of the Fe $L_{2,3}$ edges in Fig. 3a,b matches the expected interplanar spacing of the Fe/Mo-O (004) crystallographic planes. Figure 3c,d shows normalized background-subtracted SREELS images of the Fe $L_{2,3}$ edge recorded at the positive and negative positions, respectively, after PCA noise reduction. Four Fe/Mo-O (004) crystallographic planes are marked by arrows and numbers. An atomic-scale MCD image (Fig. 3e) was obtained by subtracting the SREELS image recorded at the positive position from that recorded at the negative position. Figure 3f shows MCD spectra

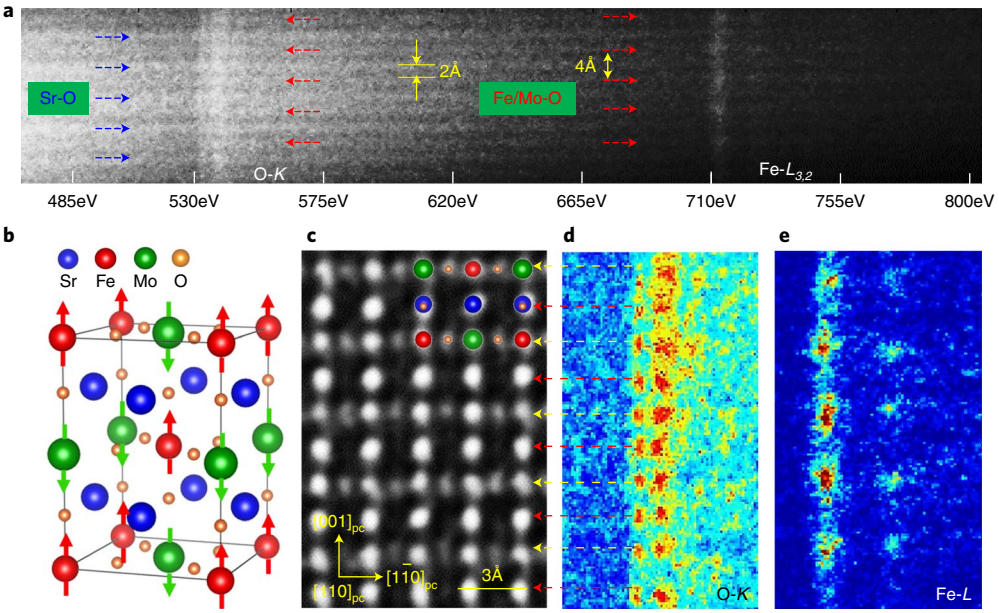

Fig. 2 | Achromatic SREELS image of SFMO. a, Raw achromatic SREELS image showing the O *K* edge and the Fe $L_{3,2}$ edge of the double perovskite SFMO in a 3BC with the (004) systematic reflections excited and without using an objective aperture. **b**, Crystallographic and magnetic structure of SFMO. The ferrimagnetically coupled spins of Fe^{3+} and Mo^{5+} cations with an ordered NaCl-type configuration are marked by the red and green arrows, respectively. **c**, Negative spherical aberration imaging of SFMO along the $[110]_{pc}$ zone axis and the corresponding projected structure model, before tilting the sample to a 3BC. **d**,**e**, Normalized background-subtracted SREELS images recorded at the O *K* edge (**d**) and the Fe $L_{3,2}$ edge (**e**) after processing using PCA.

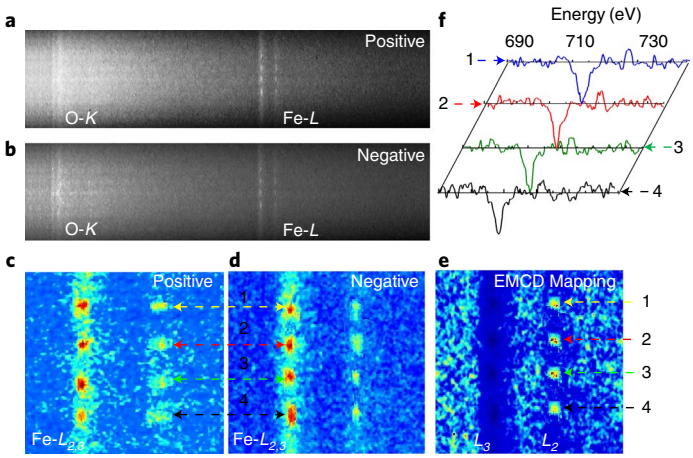

Fig. 3 | Atomic-scale imaging of magnetic circular dichroism (MCD) in SFMO. a,**b**, Achromatic SREELS images of SFMO recorded under 3BC with the (004) systematic reflections excited and the objective aperture located at the positive ('+') and negative ('−') positions, respectively. **c**,**d**, Normalized background-subtracted SREELS image of the Fe $L_{2,3}$ edge acquired at the '+' and '−' positions, respectively, and processed using PCA. **e**, Atomic-scale image of MCD achieved by subtracting the SREELS image acquired at the '+' position from that acquired at the '−' position. **f**, Experimental MCD spectra from four individual Fe/Mo-O (004) atomic planes in SFMO, as indicated by arrows in **e**. The original spectra and those after PCA processing at the position of each atomic plane are shown in Supplementary Figs. S2 and S3, respectively.

recorded from only the four individual Fe/Mo-O (004) crystallographic planes in SFMO. According to sum rules[28,29], the ratio of the spin to orbital magnetic moments (m_L/m_S) can be determined quantitatively atomic plane by atomic plane from the atomic-scale MCD image. As shown in Fig. 3e, there are at least six pixels along the vertical direction of the SREELS image for each atomic plane. Based on the six EMCD spectra per atomic plane, average values of m_L/m_S were determined at the position of each individual atomic plane, as shown in Supplementary Table S1. The resulting values of m_L/m_S are (1) 0.056 ± 0.019, (2) 0.053 ± 0.021, (3) 0.051 ± 0.020, (4) 0.058 ± 0.019, which are calculated from the MCD spectra at four atomic planes, as marked in Fig. 3e. In our previous work, the value of m_L/m_S determined by the EMCD method in standard TEM mode over a large sample area was 0.038 ± 0.01 (ref. [15]), while the value of m_L/m_S determined using XMCD is 0.033 ± 0.023 (ref. [30]). The fact that the value of m_L/m_S averaged across individual atomic planes is slightly higher than that measured using XMCD is interesting, and may result from an increase in m_L/m_S away from the centre of each atomic plane, where the contribution to a spatially averaged EMCD signal is lower.

Figure 4 shows simulations of the inelastic electron scattering cross-section, which were performed for exactly the same

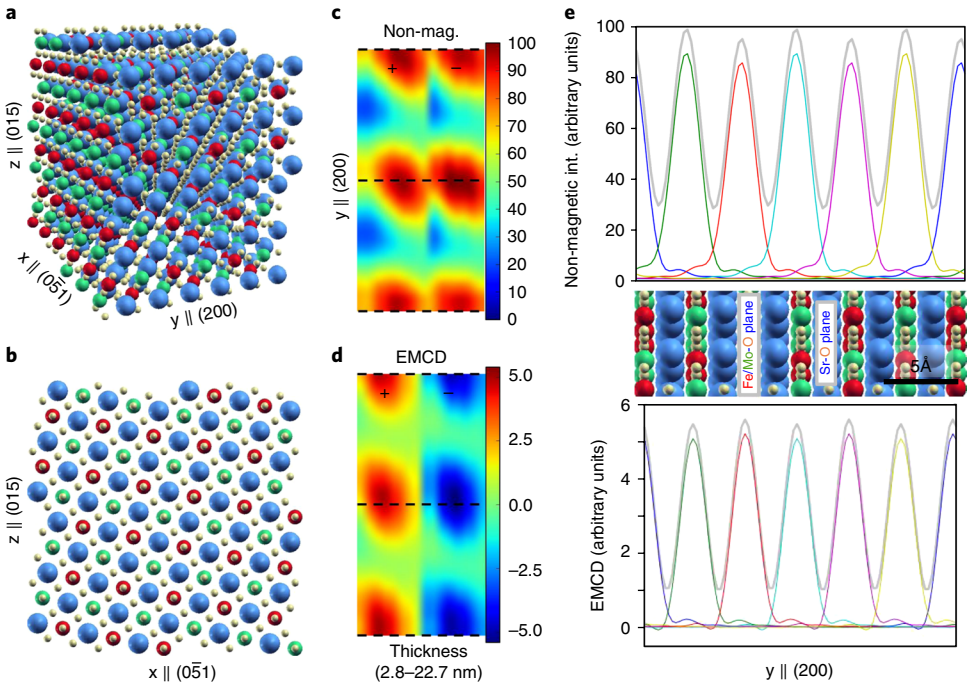

Fig. 4 | Simulations of scattering cross-sections in SREELS. a,**b**, Perspective and side views, respectively, of a structure model of SFMO in 3BC. Blue, red, green and yellow spheres represent Sr, Fe, Mo and O atoms, respectively. **c**, Non-magnetic component of the scattering cross-section for two detector orientations calculated for sample thicknesses of between 2.8 and 22.7 nm. The colour bar is in arbitrary units. **d**, Electron energy-loss magnetic chiral dichroism (EMCD) component of the scattering cross-section determined for the same conditions as in **c**, showing a different sign of the magnetic contribution for different detector orientations. The colour bar is on the same scale as in **c**. **e**, Total scattering cross-section (grey line) and individual atomic plane contributions (coloured lines) evaluated at a sample thickness of 14.2 nm. The top and bottom panels show the non-magnetic and EMCD components, respectively. The positions and compositions of the atomic planes are given in the structure model shown in the middle, which includes a scale bar for the horizontal axis. All of the simulation parameters are consistent with those used experimentally.

conditions and support the experimental findings. The non-magnetic component of the inelastic scattering cross-section shows clear contrast, allowing individual atomic planes to be resolved across the full specimen thickness range. The simulations show that the EMCD signal in the achromatic SREELS set-up at the individual detector orientations is strong, corresponding to approximately 5% of the non-magnetic signal. The optimal sample thickness is determined to be between 10 and 20 nm.

From the perspective of future applications of MCD in the SREELS configuration, it is important to understand the degree of delocalization of the contributions of individual atomic planes to the total scattering cross-section. As Fig. 4e demonstrates, the contributions from individual atomic planes (coloured lines) to the total scattering cross-section (grey line) show a remarkable degree of localization. There is negligible intermixing of the scattering cross-section contributions between neighbouring atomic planes, for both the non-magnetic and the EMCD components. The simulations therefore confirm the applicability of achromatic SREELS for the measurement of the magnetic properties of materials with atomic-plane resolution.

In summary, by combining chromatic aberration correction with SREELS, we have demonstrated atomic-scale imaging of MCD from individual Fe/Mo-O (004) atomic planes in the double perovskite SFMO under PBI conditions. In this way, the spatial resolution of MCD measurements has been improved to the atomic scale, with the m_L/m_S ratio determined quantitatively from individual atomic planes. This approach opens the door to quantify the spin configurations of individual atomic planes in epitaxial oxide heterostructures and exploring interfacial effects. It offers the possibility of achieving combined local atomic-scale magnetic, chemical and structural characterization, thereby assisting technological development and fundamental discovery in advanced magnetic materials.

Methods

Methods, including statements of data availability and any associated accession codes and references, are available at https://doi.org/10.1038/s41563-017-0010-4.

Received: 13 July 2017; Accepted: 11 December 2017;
Published online: 05 February 2018

References

1. Tokura, Y. & Nagaosa, N. Orbital physics in transition-metal oxides. *Science* **288**, 462–468 (2000).
2. Zubko, P., Gariglio, S., Gabay, M., Ghosez, P. & Triscone, J. M. Interface physics in complex oxide heterostructures. *Annu. Rev. Condens. Matter Phys.* **2**, 141–165 (2011).
3. Hwang, H. Y. et al. Emergent phenomena at oxide interfaces. *Nat. Mater.* **11**, 103–113 (2012).
4. Schattschneider, P. et al. Detection of magnetic circular dichroism using a transmission electron microscope. *Nature* **441**, 486–488 (2006).
5. Wiesendanger, R. et al. Topographic and magnetic-sensitive scanning tunneling microscopy study of magnetite. *Science* **255**, 583–586 (1992).
6. Heinze, S. et al. Real-space imaging of two-dimensional antiferromagnetism on the atomic scale. *Science* **294**, 1488–1495 (2001).
7. Kaiser, U., Schwarz, A. & Wiesendanger, R. Magnetic exchange force microscopy with atomic resolution. *Nature* **446**, 522–525 (2007).
8. Beaurepaire, E, Bulou, H, Scheurer, F. & Kappler, J. P. Magnetism and Synchrotron Radiation. (Springer: Heidelberg, 2009).
9. Chao, W. L., Harteneck, B. D., Liddle, J. A., Anderson, E. H. & Attwood, D. T. Soft X-ray microscopy at a spatial resolution better than 15nm. *Nature* **435**, 1210–1213 (2005).

10. Zhu, X. H. et al Measuring spectroscopy and magnetism of extracted and intracellular magnetosomes using soft X-ray ptychography. *Proc. Natl Acad. Sci. USA* **113**, E8219–E8227 (2016).
11. Midgley, P. A. & Dunin-Borkowski, R. E. Electron tomography and holography in materials science. *Nat. Mater.* **8**, 271–280 (2009).
12. Lidbaum, H. et al. Quantitative magnetic information from reciprocal space maps in transmission electron microscopy. *Phys. Rev. Lett.* **102**, 037201 (2009).
13. Wang, Z. Q., Zhong, X. Y., Yu, R., Cheng, Z. Y. & Zhu, J. Quantitative experimental determination of site-specific magnetic structures by transmitted electrons. *Nat. Commun.* **4**, 1395 (2013).
14. Song, D. S., Li, G., Cai, J. W. & Zhu, J. A general way for quantitative magnetic measurement by transmitted electrons. *Sci. Rep.* **6**, 18489 (2016).
15. Wang, Z. C. et al. Effects of dynamic diffraction conditions on magnetic parameter determination in a double perovskite Sr_2FeMoO_6 using electron energy-loss magnetic chiral dichroism. *Ultramicroscopy* **176**, 212–217 (2017).
16. Schattschneider, P. et al. Detection of magnetic circular dichroism on the two-nanometer scale. *Phys. Rev. B* **78**, 104413 (2008).
17. Jin, L. et al. Direct demonstration of a magnetic dead layer resulting from A-site cation inhomogeneity in a (La,Sr)MnO_3 epitaxial film system. *Adv. Mater. Interfaces* **3**, 1600414 (2016).
18. Thersleff, T., Rusz, J., Hjorvarsson, B. & Leifer, K. Detection of magnetic circular dichroism with subnanometer convergent electron beams. *Phys. Rev. B* **94**, 134430 (2016).
19. Rusz, J. et al. Magnetic measurements with atomic-plane resolution. *Nat. Commun.* **7**, 12672 (2016).
20. Rusz, J. et al. Achieving atomic resolution magnetic dichroism by controlling the phase symmetry of an electron probe. *Phys. Rev. Lett.* **113**, 145501 (2014).
21. Idrobo, J. C. et al. Detecting magnetic ordering with atomic size electron probes. *Adv. Struct. Chem. Imag.* **2**, 5 (2016).
22. Reimer, L., Fromn, I., Hirsch, P., Plate, U. & Rennekamp, R. Combination of EELS modes and electron spectroscopic imaging and diffraction in an energy-filtering electron microscope. *Ultramicroscopy* **46**, 335–347 (1992).
23. Kimoto, K., Sekiguchi, T. & Aoyama, T. Chemical shift mapping of Si L and K edges using spatially resolved EELS and energy-filtering TEM. *J. Electron Microsc.* **46**, 369–374 (1997).
24. Walther, T. Electron energy-loss spectroscopic profiling of thin film structures: 0.39 nm line resolution and 0.04 eV precision measurement of near-edge structure shifts at interfaces. *Ultramicroscopy* **96**, 401–411 (2003).
25. Kabius, B. et al. First application of *Cc*-corrected imaging for high-resolution and energy-filtered TEM. *J. Electron Microsc.* **58**, 147–155 (2009).
26. Urban, K. W. et al. Achromatic elemental mapping beyond the nanoscale in the transmission electron microscope. *Phys. Rev. Lett.* **110**, 185507 (2013).
27. Forbes, B. D., Houben, L., Mayer, J., Dunin-Borkowski, R. E. & Allen, L. J. Elemental mapping in achromatic atomic-resolution energy-filtered transmission electron microscopy. *Ultramicroscopy* **147**, 98–105 (2014).
28. Calmels, L. et al. Experimental application of sum rules for electron energy loss magnetic chiral dichroism. *Phys. Rev. B* **76**, 060409 (2007).
29. Rusz, J., Eriksson, O., Novák, P. & Oppeneer, P. Sum rules for electron energy loss near edge spectra. *Phys. Rev. B* **89**, 134428 (2014).
30. Koide, T. et al. Microscopic origin of ferrimagnetism of a double perovskite Sr_2FeMoO_6: an X-ray magnetic circular dichroism study. *J. Phys. Conf. Ser.* **502**, 012003 (2014).

Acknowledgements

This work was supported by the National Key Research and Development Program (2016YFB0700402), the National Natural Science Foundation of China (51671112, 5171101391, 51471096, 11374174, 51390471, 51527803, 51525102, 51390475, 51371102), the National Basic Research Program of China (2015CB921700, 2015CB654902), Tsinghua University (20141081200), National Key Scientific Instruments and Equipment Development Project (2013YQ120353) and the "Strategic Partnership RWTH-Aachen University and Tsinghua University" Program. R.D.-B. is grateful for funding from the European Research Council under the European Union's Seventh Framework Programme (FP7/2007-2013)/ ERC grant agreement number 320832. This work made use of resources in Forschungszentrum Jülich, Germany and the National Center for Electron Microscopy in Beijing, China. J.R. acknowledges the Swedish Research Council and Göran Gustafsson's Foundation for financial support. Calculations were performed using the Swedish National Infrastructure for Computing (SNIC) on a Triolith cluster at the National Supercomputer Center (NSC) of Linköping University. L. Houben, C.-L. Jia, M. Lentzen, M. Luysberg, C. B. Boothroyd, A. Schwedt, D. Meertens, M. Kruth, M. Duchamp, E. Kita, H. Yanagihara, P. Ercius, C. Kisielowski, F.-R. Chen, M. Linck, H. Müller and M. Haider are gratefully acknowledged for helpful discussions and assistance.

Author contributions

X.Y.Z. initiated the idea and developed the principles. Z.C.W. prepared the TEM samples, performed HRTEM/STEM experiments, processed the experimental data under the supervision of L.J. and X.Y.Z., and drafted the manuscript. A.T., L.J. and X.Y.Z. carried out achromatic atomic-scale SREELS and EMCD measurements in Jülich. J.R. and D.T. carried out theoretical simulations of atomic-scale mapping of MCD. R.Y. and J.Z. participated in the development of the principles and experimental design. Y.M. provided the bulk sample. J.M., R.D.-B., R.Y. and J.Z. contributed to the scientific discussions. All of the authors participated in discussions and writing the manuscript.

Competing interests

The authors declare no competing financial interests

Additional information

Supplementary information is available for this paper at https://doi.org/10.1038/s41563-017-0010-4.

Reprints and permissions information is available at www.nature.com/reprints.

Correspondence and requests for materials should be addressed to X.Z.

Publisher's note: Springer Nature remains neutral with regard to jurisdictional claims in published maps and institutional affiliations.

Methods

Material and sample preparation. The polycrystalline Sr_2FeMoO_6 (SFMO) was melt-grown in a floating-zone furnace using the raw materials MoO_3, Mo, Fe_2O_3 and $SrCO_3$. The samples were extruded into a rod of size 5 mm diameter × 50 mm length and sintered at 1200 °C for 2 h in an Ar atmosphere with a feed speed of ~20 mm h^{-1} (ref. [15]). The TEM specimens, consisting of single-crystal grains with the desired crystallographic orientations, were prepared from polycrystalline SFMO with grain sizes of up to 60μm by focused ion beam milling and traditional methods.

The ferrimagnetic double perovskite SFMO has a Curie temperature of ~420 K and a tetragonal structure with lattice parameters $a = b = 5.56850$ Å, $c = 7.89722$ Å (ref. [31]), as shown in Fig. 2b. The origin of ferrimagnetism in SFMO is attributed to antiferromagnetic super-exchange between the spins of Fe^{3+} and the spins of Mo^{5+} cations with an ordered NaCl-type configuration[32]. In order to fulfill the requirements for EMCD detection of the M_z component, the soft magnet SFMO samples[33] with an anisotropy constant K_1 of 28 kJ m^{-3} get saturated along the incident electron beam direction at any sample tilt angle under the ~2 T magnetic field provided by the TEM objective lens.

Data acquisition. TEM, EELS and EMCD measurements were carried out on an FEI Titan G3 50-300 PICO fourth-generation TEM, which is capable of recording high-resolution TEM images with a spatial resolution of ~50 pm. The microscope is equipped with a Schottky-type high-brightness electron gun (FEI X-FEG), a monochromator, a C_S probe corrector (CEOS DCOR), a C_S-C_C achro-aplanat image corrector (CEOS CCOR+), a post-column imaging energy filter (Gatan Quantum 966 ERS) and a 16-megapixel CCD camera (Gatan UltraScan 4000 UHS)[34]. The sample was tilted to a 3BC with an (004) systematic row excited and with the electron beam strictly parallel to the (004) crystallographic planes. The beam semi-convergence angle was 4.12 mrad and the detector semi-collection angle was 5.76 mrad. The OA was placed at the positive and negative positions in the back focal plane, as shown in Fig. 1c. The C_C and C_S values were set to 516 nm and -5.38 μm, respectively. The acquisition times for SREELS images of SFMO without an OA for atomic-scale EELS and with an OA inserted for atomic-scale EMCD were 5 and 30 s, respectively. The atomic-scale EMCD experiments were performed more than 70 times over different thin areas in individual single-crystalline grains of polycrystalline Sr_2FeMoO_6 with grain sizes of several tens of micrometres.

Data analysis. EELS data processing included pre-edge background subtraction and removal of plural scattering using Fourier-ratio deconvolution with a zero-loss modifier function. Atomic-resolution SREELS images were processed using PCA (ref. [35]). The '+' and '−' SREELS images were background-subtracted by integrating the intensity in a pre-edge window between 620 and 680 eV using Cornell Spectrum Imager (CSI) software[36] and normalized by integration of the intensity in a post-edge window. EMCD signals were obtained by subtracting the two SREELS images from each other. As shown in Supplementary Fig. S2, even without any PCA processing the EMCD signals of the Fe L_3 and L_2 edges at four individual atomic planes are well resolved when compared to the noise level.

Theoretical simulations. For simulations, orthogonal supercells of SFMO were constructed with the c axis along [015] and the y axis along [200]. Minimal supercell dimensions in multislice simulations were 2.83 × 0.79 × 2.83 nm sampled on a 440 × 128 × 400 pixel grid. For inelastic scattering simulations, a combined multislice/Bloch-wave method[37,38] was adapted for SREELS with a convergence parameter of 5×10^{-7}. When evaluating the delocalization of inelastic scattering, the minimal orthogonal supercell was tripled along the y direction so that the contributions of six individual Fe-Mo-O planes could be evaluated. For the simulation, the beam semi-convergence angle was 4.12 mrad and the detector semi-collection angle was 5.76 mrad. All of the parameters used in the simulations were consistent with those used in the experiments.

Data availability. The authors declare that the data supporting the findings of this study are available within the paper and its supplementary information files.

References

31. Kobayashi, K.-I., Kimura, T., Sawada, H., Terakura, K. & Tokura, Y. Room-temperature magnetoresistance in an oxide material with an ordered double-perovskite structure. *Nature* **395**, 677–680 (1998).
32. Moritomo, Y. et al. Crystal and magnetic structure of conducting double perovskite Sr_2FeMoO_6. *J. Phys. Soc. Jap* **69**, 1723–1726 (2000).
33. Serrate, D., De Teresa, J. M. & Ibarra, M. R. Double perovskites with ferromagnetism above room temperature. *J. Phys. Condens. Matter* **19**, 023201 (2007).
34. Barthel, J., Houben, L. & Tillmann, K. *J. Large-Scale Res. Facil.* **1**, A34 (2015).
35. Varela, M. et al. Atomic-resolution imaging of oxidation states in manganites. *Phys. Rev. B* **79**, 085117 (2009).
36. Cueva, P. C., Hovden, R., Mundy, J. A., Xin, H. L. & Muller, D. A. Data processing for atomic resolution electron energy loss spectroscopy. *Microsc. Microanal.* **18**, 667–669 (2012).
37. Rusz, J., Bhowmick, S., Eriksson, M. & Karlsson, N. Scattering of electron vortex beams on a magnetic crystal: Towards atomic-resolution magnetic measurements. *Phys. Rev. B* **89**, 134428 (2014).
38. Song, D. S., Wang, Z. Q. & Zhu, J. Effect of the asymmetry of dynamical electron diffraction on intensity of acquired EMCD signals. *Ultramicroscopy* **148**, 42–51 (2015).